Microstructural analysis of simulated liquid and amorphous Ni

Alvaro Posada-Amarillas
Programa de Posgrado en Física de Materiales, Centro de Investigación Científica y de Educación Superior de Ensenada, Apartado Postal 2681, Ensenada, Baja California, 22800 Mexico
and Centro de Investigación en Física, Universidad de Sonora, Apartado Postal 5-088, Hermosillo, Sonora, 83000 Mexico

Ignacio L. Garzón
Instituto de Física, Universidad Nacional Autónoma de México, Apartado Postal 2681, Ensenada, Baja California, 22800 Mexico
(Received 26 October 1995)

Molecular dynamics simulations and a systematic analysis of the local atomic structure have been done to investigate the microstructure of liquid and amorphous Ni. The n-body Gupta potential, based on the second moment approximation of a tight-binding Hamiltonian, was used to model the metallic bonding of the system. The calculated pair distribution function (PDF) of liquid and amorphous Ni are in agreement with experimental measurements. A decomposition of the first and second peaks of the PDF into components according to the local environment of the pairs shows that the atomic coordination of the liquid phase contains a high abundance of icosahedral and distorted icosahedral structures. Crystalline and icosahedral (regular and distorted) atomic configurations contribute in approximately the same proportion to the short-range order of the amorphous phase. These results indicate that n-body interactions favor the formation of crystalline order in amorphous metals.

I. INTRODUCTION

A knowledge of the physical and chemical behavior of non-crystalline transition metals is essential to optimize several metallurgy industrial processes (liquids) and to understand their exciting properties like high values of hardness, strength and corrosion resistance (amorphous). In particular, the study of structural properties of liquid and amorphous transition metals has been a very active field of research,[1–3] both theoretically and experimentally. One interesting question in liquid-state physics is whether the liquid structure of transition and noble metals, having incomplete d or f electronic shells, differs from that of simple metals such as aluminum. According to experimental data,[1] although these materials have incomplete d and f shells, their structure factors can be put into the same class as simple metals. This experimental fact gives a surprisingly simple description for the structure of most liquid transition and noble metals.[1] Theoretical studies on the structure of these systems are based on semiempirical approaches like embedded-atom method (EAM) (Refs. 4 and 5), and more recently, on first principles calculations (Car and Parrinello method for liquid Cu).[6] Good agreement between calculated and experimental structure factors and pair distribution functions (PDF's) have been found for several liquid transition and noble metals.[4–6]

A comparison between the structural properties of amorphous and liquid transition metals shows that the general features in the structure of the amorphous phase, are similar to those of the liquid state, except for a shoulder in the second peak observed in both the structure factor, $S(k)$, and the PDF, $g(r)$.[1] A typical example of this difference is found in Ni, which shows a clear splitting of the second peak in $S(k)$ and $g(r)$ [see Figs. 1(a) and 1(b)], when it is in the amorphous state.[1,7] Several models of disordered structures have been proposed to describe and reproduce the basic profiles of the structure factor and PDF observed experimentally.[1,2] In particular, the modified dense random packing model of hard spheres (DRPHS) (Ref. 8) and the dense random packing model of Lennard-Jones (LJ) ''atoms'' (DRPLJ) (Ref. 9) describe, qualitatively, the splitting

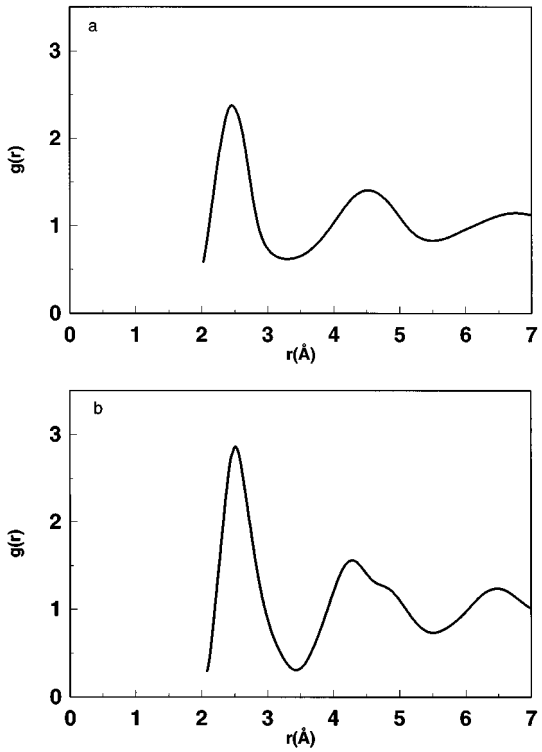

FIG. 1. Experimental pair distribution function of (a) liquid Ni at $T=2020$ K; (b) amorphous Ni at low temperature. The data are taken from Ref. 1 (liquid) and Ref. 7 (amorphous).

mechanism in the PDF second peak of amorphous systems, in terms of the formation of special atomic configurations with relative dominant contributions.

An insightful approach to study the local structure of liquid and amorphous states of matter is through the classification of atomic configurations, according to multidimensional potential energy minima, that can be reached by steepest-descent paths in computer simulations of these systems.[10,11] This ''inherent structure'' formalism is a way of partitioning the configuration space for the vibrations of a n-body system into various regions. Within each region there is one local minimum of the potential energy surface which can be reached by a minimization algorithm. This process is the basis for the partitioning of configuration space and the structure at the local minimum is the inherent structure of the corresponding region. The idea of resolving observable order in liquid and amorphous materials into vibrational and inherent structural parts offers a way to classify their microstructure and discover the kind of short-range order present in these materials.

The above approach has been used to study the microstructure of clusters, liquids and amorphous model systems using the LJ potential,[9,12–14] and the common-neighbor analysis (CNA) (Ref. 15) to systematically classify the abundance of inherent structures characteristic of these systems. It was found that a LJ liquid contains inherent structures with local fivefold symmetry, characteristic of icosahedral order.[12,13] The abundance of such structures is temperature independent at high temperatures, but slightly above the glass transition temperature the LJ glass shows an increase in abundance of icosahedral structures with a decrease at the same time, of configurations characteristic of fcc and hcp crystalline phases. Local icosahedral order has also been found when the density of random hard-sphere packing increases[9] or in the pressure-induced glass transition of a LJ system.[14]

In other computer simulation studies, using a nonadditive LJ potential and Voronoi polyhedra analysis,[16] it was found that in an amorphous Ni-Y alloy the atomic coordination resembles that of the crystalline species with very small presence of icosahedral structures. It was pointed out[17] that the scarcity of icosahedral clusters should be attributed to the large nonadditivity of the interatomic forces: if nonadditivity is reduced icosahedral order increases.

In this work, we present results of a microstructural study of liquid and amorphous nickel using molecular dynamics simulations and steepest-descent method to find the inherent structures of the multidimensional potential energy surface given by a n-body Gupta potential, adequate to model the metallic bonding. The main objective of the present work is to investigate the kind of short-range order present in the local environment of a transition metal in liquid and amorphous phases, using a n-body potential interaction. A decomposition of the first and second peaks of the PDF, using a method to systematically classify the inherent structures, will allow us to characterize the local order to gain additional insight into the structural properties of noncrystalline transition metals. In Sec. II, we present the model potential and computational details used in this simulation. Section III contains the results and a discussion of them. A brief summary and the conclusions of this work are given in Sec. IV.

II. COMPUTATIONAL DETAILS

A. Model potential

The metallic bonding of noncrystalline Ni is modeled through a n-body potential that is based on Gupta's expression[18] for the cohesive energy of transition and noble metals. The attractive term of the interatomic interaction is based on the second moment approximation of a tight-binding Hamiltonian in which n-body effects are included. The repulsive part is a sum of pairwise Born-Mayer potentials. As a function of the interatomic distance r_{ij}, it is written as

$$V=\frac{U}{2}\sum_{j=1}^{n}\left[A\sum_{i(\neq j)=1}^{n}\exp[-p(r_{ij}/r_0-1)]-\left[\sum_{i(\neq j)=1}^{n}\exp[-2q(r_{ij}/r_0-1)]\right]^{1/2}\right], \qquad (1)$$

where the parameters U, A, p, q, and r_0 depend on the material. In this work we adopt the values $p=9$ and $q=3$, which have been used for transition metals.[19] The value $A=0.101\,036$ is obtained when the cohesive energy of the fcc metal at the equilibrium value of its nearest-neighbor distance converged. The $U=3.40$ eV and $r_0=2.49$ Å values were used after fitting the calculated lattice constant and cohesive energy to the experimental values of bulk fcc Ni. The Gupta potential given in Eq. (1) has been used to study structural and thermodynamical properties of fcc (Refs. 20 and 21) and hcp transition metals and alloys.[21] The ability of this potential to describe real materials has been tested by calculating point-defect properties, lattice dynamics and finite temperature behavior, and by comparing the results with other potential schemes.[21] Structural, dynamical,[22–24] vibrational,[25] and fragmentation[26] properties of metal clusters have been extensively studied using the Gupta n-body potential in molecular dynamics simulations. The effect of the n-body interaction on the physical behavior of metal clusters is shown through their structural and dynamical properties when they are compared with results coming from pairwise interactions.[22–24] In this work, we extend the range of applications of this potential exploring its capability to describe structural properties of noncrystalline transition metals (Ni in this case).

B. Molecular dynamics and inherent structures

Molecular dynamics (MD) simulations at constant total energy were performed on a system of 256 particles using periodic boundary conditions. The Newton's equations of motion were solved using the Verlet algorithm[27] with a time step of 7.8×10^{-16} s. This time step assures conservation of total energy, even in the longest run (10^5 time steps), within 0.5%. The initial values of the atomic coordinates corresponded to a fcc lattice and the initial momenta were chosen from a Maxwell-Boltzmann distribution of velocities. From this initial configuration, the system was equilibrated and then heated up in a steplike manner scaling the atom velocities up to a temperature beyond the melting point. The mean-square-displacement as a function of time was calculated to monitor the degree of diffusional motion of the system. At a

temperature close to the melting point the calculated diffusion coefficient was 0.40×10^{-4} cm^2/s. This value compares well with those obtained in MD simulations of liquid Ni using EAM potentials:[28,29] 0.385×10^{-4} cm^2/s and 0.391×10^{-4} cm^2/s. For liquid Ni no experimental values of the diffusion coefficient are known. Once the liquid state was reached, a run of about 80 ps was done at $T=2000$ K to calculate its structural properties. During this MD run the steepest-descent method was coupled,[30] eliminating the effect of thermal motion, to determine a series of independent inherent structures, characteristic of the liquid state.

The simulated amorphous sample was obtained using a fast quench from the liquid phase at $T=2000$ K to a low temperature state, at a cooling rate of $\sim10^{12}$ K s^{-1}. Having reached a temperature of 100 K, the system was let free to evolve for 10 ps. In order to better stabilize the structure, the system was led to an annealing cycle during which, the temperature was raised to 700 K and then allowed to evolve for 10 ps. The temperature was reduced again to 100 K and then the system was equilibrated. After annealing, the system was allowed to evolve for about 80 ps during which temporal averages were taken. The effects of the quenching rate and annealing on the amorphous structure and properties have been studied before,[31] indicating that the glass transition temperature increases with the cooling rate. The quenching-annealing procedure described above was used in the amorphization of materials like Ni,[31] Si,[32] and Ge.[33] A good agreement of the calculated structural properties with experimental data was obtained, indicating that this process is effective to generate amorphous simulated samples. Inherent structures of amorphous Ni were obtained during the MD run at $T=100$ K, using the steepest-descent method to suppress vibrational motion effects, in the same way as it was done for the liquid phase.

III. RESULTS AND DISCUSSION

A. Structural properties

Using the atomic coordinates of the configurations collected during the MD simulation, we obtain the pair distribution function $g(r)$ of liquid and amorphous Ni. They are displayed in Figs. 2(a) and 2(b), respectively. A comparison with the experimental curves of Figs. 1(a) and 1(b) show a good agreement in the overall shape. In the liquid case, Fig. 2(a), the calculated $g(r)$ at $T=2000$ K, shows a symmetric first peak with its maximum at a position $r_1=2.34$ Å. The second maximum is placed at $r_2=4.36$ Å, giving a ratio $r_2/r_1=1.86$, characteristic of simple liquid metals and in agreement with the experimental value.[1] Although the ratio r_2/r_1 is well reproduced, the peak positions are shifted by about 5% to lower values than those reported experimentally.[1] This difference is expected since the potential parameters were not optimized to obtain a perfect agreement with experimental data. It is notorious, however, that the main properties of the PDF for liquid Ni can be obtained from the Gupta n-body potential, extending its range of applications to liquid metal systems. A better agreement with experimental values is expected if we use a set of parameters obtained through a more complex optimization procedure.[21]

The calculated PDF of amorphous Ni is shown in Fig. 2(b). It clearly shows the main characteristic of a metallic glass: the splitting of the second peak. The first peak is symmetric and its maximum is located at $r_1=2.40$ Å. The two splitted subpeaks are at $r_2=4.22$ Å and $r_3=4.70$ Å, giving ratio values of $r_2/r_1=1.76$ and $r_3/r_1=1.96$, respectively. The comparison of these values with experimental results[1] ($r_2/r_1=1.71$ and $r_3/r_1=1.95$) indicates that the calculated subpeaks are slightly shifted to larger distances. Although the overall shape of the calculated PDF is in agreement with the experimental curve reported by Ichikawa,[7] shown in Fig. 1(b), they differ in the heights of the first peak. This difference could be associated to a possible higher temperature value of the experimental sample with respect to the simulated one.

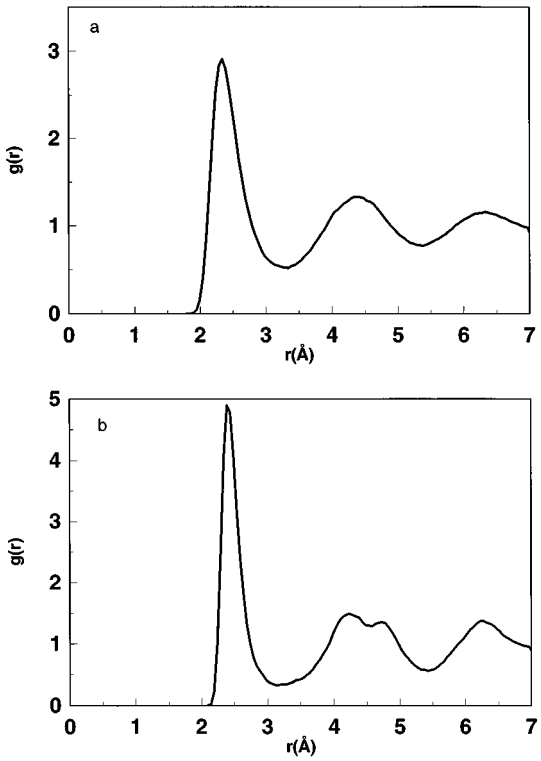

FIG. 2. Calculated pair distribution function for (a) liquid Ni at $T=2000$ K; (b) amorphous Ni at $T=100$ K.

A widespread interpretation of the characteristic shape of the PDF for amorphous metals associates the short-range order of near neighbors with the atomic arrangement of the crystalline state.[1] However, from the similarity in $g(r)$, the fundamental configuration of atoms in the amorphous state should be considered as liquidlike. Several models of disordered structures, like the microcrystalline disordered model and the topological disorder model have been used to get insight into the atomic configurations of amorphous metals.[1] The topological disorder model based on the dense random packing of hard spheres (DRPHS), extended by Ichikawa,[8] suggests the formation of distorted tetrahedrons as the fundamental units of a close-packed disordered atomic distribution. This distribution is relatively distinct in comparison with that of liquids, being the packing more rigid in the amorphous state than in the liquid one. This model explains qualitatively the splitting of the second peak in $g(r)$ for the amorphous phase and the absence of it for the liquid one. In the next subsection, we describe a method to systematically

analyze the microstructure of liquid and amorphous Ni through the classification of their inherent structures. This procedure will allow us to obtain the atomic configurations that generate the characteristic short-range order in these noncrystalline materials.

B. Microstructural analysis

In the past subsection we have shown that the n-body Gupta potential reproduces quite well structural properties of liquid and amorphous Ni. This resemblance between theory and experiments suggests that a similar resemblance should exist between the simulated atomic configurations and the real noncrystalline material. To obtain a detailed three-dimensional description of the local atomic configuration, we used a method to classify the inherent structures resulting after applying a steepest-descent minimization technique to liquid and amorphous configurations at 2000 and 100 K, respectively. This method is able to decompose the first and second peaks of the PDF by characterizing the local environment surrounding each atomic pair that contributes to the peaks of $g(r)$, in terms of the number and properties of common nearest neighbors of the pair under consideration. The earlier version of this method was introduced to analyze three-body effects on the energy of small clusters[34] and then extended to study structural properties of one-component LJ clusters[12] and structural relaxations in one- and two-component LJ liquids.[13] Recently, Faken and Jónsson,[15] generalized such a method, introducing the common neighbor analysis (CNA) method to systematically analyze the local atomic structure in combination with three-dimensional (3D) computer graphics.

In this work, we use the common-neighbor method as implemented by Blaisten-Barojas,[34] assigning to each atomic pair, contributing to the PDF, a set of four indices under the following criterion. (i) The first index denotes to what peak of the PDF belongs the pair under consideration. (ii) The second index counts the number of common nearest-neighbors of that pair. (iii) The third index specifies the number of nearest-neighbor bonds found between the number of particles denoted by the second index. (iv) A fourth index sometimes is necessary to distinguish configurations with the same first three indices but being topologically different. The position of the first and second minima of the PDF are used as a cutoff distance to define the nearest-neighbor and second nearest-neighbor particles, respectively. This method is able to distinguish between various local structures like fcc, hcp, bcc, and icosahedral environments. Different types of pairs are associated to different types of local order. For example, fcc order only have pairs of the type 1421, whereas the hcp crystal has equal number of 1421 and 1422 pairs. The difference between 1421 and 1422 pairs is the topological arrangement of the two bonds between the four neighbors. The pair 1551, corresponding to a pentagonal bipyramid, is characteristic of icosahedral order. Figures 3(a) and 3(b) show the atomic configurations of inherent structures more frequently obtained after using the above method. The structures shown in Fig. 3(a) correspond to pairs of the first peak and those shown in Fig. 3(b) are coming from the second one.

Tables I and II show the normalized abundance of selected pairs at three different times during the MD run and the corresponding average for liquid and amorphous Ni, respectively. The quantities are normalized such that the total number of pairs contributing to the first peak of the PDF is unity. The first PDF peak of liquid Ni is mainly due to 1551, 1541, and 1431 pairs. The last two pairs (1541 and 1431) are formed when regular 1551 structures deformed, if a bond is broken.[9] Therefore, their presence is an indication of the existence of distorted icosahedral order. The contribution of 1551 pairs, corresponding to fivefold symmetry structures, is 27% of the total contribution to the first peak, whereas an equal proportion is due to 1541 and 1431 pairs producing deformed fivefold structures. fcc structures are present through the existence of 1421 pairs, but only in a small proportion ($\sim 4\%$).

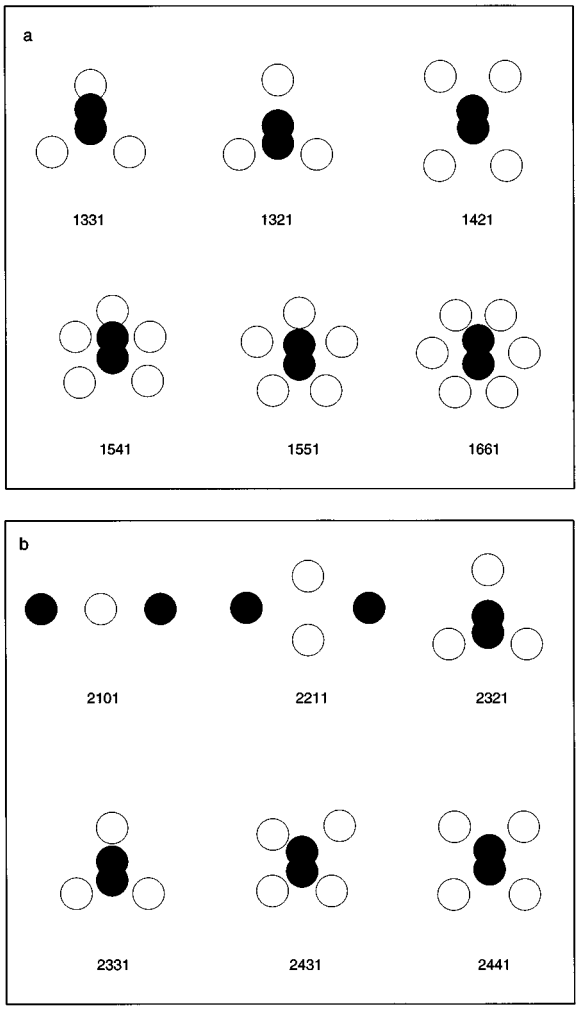

FIG. 3. Atomic configurations of inherent structures corresponding to (a) the first peak of the PDF and (b) the second peak of the PDF. The pair is shown with dark circles. The open circles represent their common neighbors which define the local environment of the pair. The four indices given below specify each configuration.

Three types of pairs (2101, 2211, and 2331) are the main components of the second peak of the PDF. The relative high proportion of the 2331 pair, characteristic of pentagonal bipyramid structures, confirms the presence of atomic configurations with fivefold symmetry in liquid Ni. Since the pairs corresponding to inherent structures with pentagonal symmetry (regular and distorted) are the more abundant in the first and second peaks of the PDF, the short-range order in liquid

TABLE I. Normalized abundance of inherent structures for liquid Ni at $T=2000$ K, calculated at three different times, using steepest-descent method and the atomic configurations obtained during the MD run. The average was calculated using the values shown in the first three columns. Data for less abundant structures are not shown.

Pair	$t=25$ ps	$t=50$ ps	$t=75$ ps	Average
1321	0.03	0.01	0.02	0.02
1421	0.03	0.05	0.04	0.04
1431	0.13	0.14	0.12	0.13
1541	0.13	0.15	0.15	0.14
1551	0.25	0.25	0.32	0.27
1661	0.14	0.14	0.14	0.14
2101	1.01	1.06	1.09	1.06
2211	1.05	1.02	0.97	1.02
2321	0.09	0.08	0.06	0.07
2331	0.78	0.82	0.88	0.83
2431	0.01	0.01	0.01	0.01
2441	0.05	0.07	0.07	0.06

Ni is dominated by local icosahedral order. Local icosahedral order means order characteristic of a 13 atom icosahedron, namely the presence of 1551 and 2331 pairs and absence of 1421, 1422, and 2441 pairs (typical of fcc and hcp structures). A system with local icosahedral structure need not contain a complete 13 atom icosahedron, but only the principal structural motifs characteristic of the icosahedron.[12] Then, the microscopic picture emerging from the present analysis indicates that the short-range order of liquid Ni is dominated by icosahedral and distorted icosahedral inherent structures. Similar results were found for the microstructure of a LJ liquid.[12] This agreement suggests that not only the overall shape and peak positions ratio of the PDF for liquid transition metals like Ni coincide with those of simple liquids, but also the local atomic configuration of the liquid microstructure.

The amorphous Ni microstructural analysis is resumed in Table II. It shows that the first peak of the PDF is composed mainly of 1551, 1541, 1431, and 1421 pairs, all of them in approximately the same proportion ($\sim 20\%$). As we have seen, 1551 pairs are associated to pentagonal bipyramids forming icosahedral structures, whereas pairs of the type 1541 and 1431 are characteristic of distorted icosahedral order. The presence of 1421 pairs indicate that in the local atomic structure of amorphous Ni, crystalline short-range order exists and, according to the data of Table II, in a proportion comparable to icosahedral and distorted icosahedral order. Our data shows that as a result of the amorphization process the amount of icosahedral and distorted icosahedral order present in liquid Ni reduce in favor of the formation of crystalline order. This effect is not obvious since the first peak of the PDF in liquid and amorphous Ni are similar. However, the microstructural analysis allows us to discover the formation of crystalline atomic configurations through the increase in the abundance of 1421 pairs in the amorphous sample with respect to the liquid one. This increment of crystalline order after amorphization was not observed in simulations done for LJ systems.[12,13] Instead, fivefold structures became more abundant and a slight decrease of crystalline structures was observed. The origin of this difference has been attributed to the effects of nonadditive forces:[17] more icosahedral structures are present when nonadditivity is reduced. A molecular dynamics simulation for amorphous Ni-Y alloys[16] using a nonadditive LJ potential indicated that atomic coordination in the simulated glass resembles that of the crystalline species and icosahedral clusters are quite rare. In the present work, we are using a Gupta potential which includes n-body terms in the attractive part of the interaction. The nonadditivity of this potential has been effective in explaining the experimentally observed contraction of the first layer of transition metal surfaces[18] and the Cauchy discrepancy: $C_{12} \neq C_{44}$.[19] Therefore, our results support the idea that nonadditive forces due to n-body potentials favor the formation of crystalline short-range order and at the same time reduce the content of icosahedral order in amorphous transition metals.

TABLE II. Same as Table I for amorphous Ni at $T=100$ K.

Pair	$t=25$ ps	$t=50$ ps	$t=75$ ps	Average
1321	0.01	0.01	0.01	0.01
1421	0.21	0.22	0.21	0.21
1431	0.21	0.22	0.22	0.22
1541	0.25	0.23	0.24	0.24
1551	0.21	0.18	0.17	0.18
1661	0.04	0.05	0.05	0.05
2101	1.51	1.50	1.51	1.51
2211	1.02	1.07	1.05	1.05
2321	0.07	0.08	0.08	0.08
2331	0.77	0.73	0.71	0.74
2431	0.02	0.02	0.03	0.02
2441	0.17	0.22	0.17	0.19

Other application of the present microstructural analysis is the decomposition of the second peak of the PDF for amorphous Ni. Table II shows the percentage of pairs with the highest relative abundance. A comparison with the data corresponding to liquid Ni indicates the increase of 2101 pairs after amorphization. This type of pairs are linear trimers that are present in either crystalline (fcc or hcp) or icosahedral structures. Since the data for the first peak shows that fivefold symmetry structures reduce upon fast quenching, these pairs should be related to crystalline structures. The reduction in the abundance of 2331 pairs is consistent with the decrease of icosahedral structures for the amorphous phase. In contrast, the increment in the relative abundance of 2441 pairs in the amorphous state with respect to the liquid one, confirms the formation of crystalline structures as was found from the microstructural analysis of the first peak of the PDF.

To explore the splitting mechanism of the PDF second peak, in terms of the formation of special inherent structures, we have plotted in Fig. 4 the partial contributions of $g(r)$ due to the more abundant types of pairs. It is found that pairs type 2210 and 2331 are giving the main contributions to the first subpeak, whereas the second subpeak clearly arises from the 2101 pair. Therefore, the splitting of the second peak in

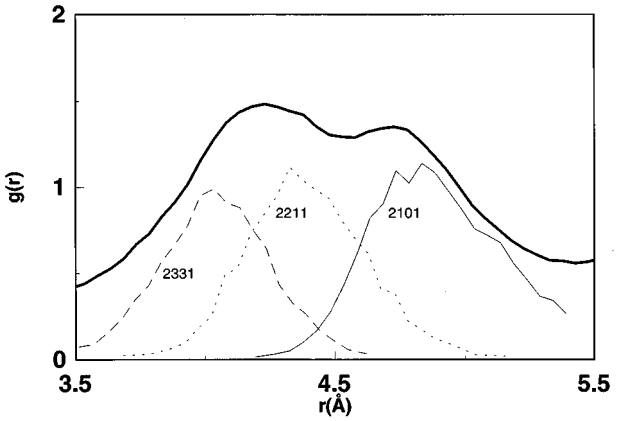

FIG. 4. Partial components of the second PDF peak for amorphous Ni (averaged over three atomic configurations). Solid thick line, total PDF; solid thin line, the 2101 component; short-dashed line, the 2211 component; large-dashed line, the 2331 component.

the amorphous Ni PDF is mainly due to the formation of specific inherent structures distributed around a characteristic range of distances. In the pairs type 2210 and 2331 the distribution of the atom-atom distances in the seed pair is in the region underlying the first subpeak. The corresponding distribution due to pairs type 2101 is centered at larger distances giving the main contribution to the second subpeak. Since the abundance of 2101 pairs is larger in the amorphous phase, the PDF has a splitted second peak. In the liquid state, the abundance of these pairs is not enough to see such effect. These results are consistent with those obtained by Ichikawa[8] using a modified DRPHS model, for amorphous Ni, and by Clarke and Jónsson[9] for a LJ glass.

IV. CONCLUSIONS

We have presented a constant-energy MD simulation study of liquid and amorphous Ni, using a Gupta n-body potential to describe the metallic bonding in the system. The noncrystalline structure of the liquid and amorphous metallic states, characterized through the PDF, was found in agreement with experimental data. A microstructural analysis, using a method to classify inherent structures, allows us to make a decomposition of the PDF to gain additional insight into the atomic configurations characterizing the noncrystalline states of Ni. The classification of inherent structures obtained for liquid Ni indicates that the short-range order is due to icosahedral and distorted icosahedral structures. The microstructure of amorphous Ni is characterized by the presence of icosahedral (regular and distorted) and crystalline order. The present study supports the idea that n-body interactions, like those existing in metallic systems, generates crystalline order at the expenses of icosahedral order characteristic of the liquid state, during the amorphization process.

ACKNOWLEDGMENTS

This work was supported by the Supercomputer Center DGSCA-UNAM, DGAPA-UNAM Project IN108296 and CONACYT-México under Project 4021-E. A.P.A. acknowledges financial support from CONACYT-México.

[1] Y. Waseda, *The Structure of Non-Crystalline Materials; Liquids and Amorphous Solids* (McGraw-Hill, New York, 1980).
[2] S.R. Elliot, *Physics of Amorphous Materials* (Longman, London, 1984).
[3] T. Iida and R.I.L. Guthrie, *The Physical Properties of Liquid Metals* (Clarendon, Oxford, 1988).
[4] S.M. Foiles, Phys. Rev. B **32**, 3409 (1985).
[5] L.M. Holzman, J.B. Adams, S.M. Foiles, and W.N.G. Hitchon, J. Mater. Res. **6**, 298 (1991).
[6] A. Pasquarello, K. Laasonen, R. Car, C. Lee, and D. Vanderbilt, Phys. Rev. Lett. **69**, 1982 (1992).
[7] T. Ichikawa, Phys. Status Solidi A **19**, 707 (1973).
[8] T. Ichikawa, Phys. Status Solidi A **29**, 293 (1975).
[9] A.S. Clarke and H. Jónsson, Phys. Rev. E **47**, 3975 (1993).
[10] F.H. Stillinger and T.A. Weber, Phys. Rev. A **25**, 978 (1982).
[11] F.H. Stillinger and T.A. Weber, Phys. Rev. A **28**, 2408 (1983).
[12] J.D. Honeycutt and H.C. Andersen, J. Phys. Chem. **91**, 4950 (1987).
[13] H. Jónsson and H.C. Andersen, Phys. Rev. Lett. **60**, 2295 (1988).
[14] S.L. Shumway, A.S. Clarke, and H. Jónsson, J. Chem. Phys. **102**, 1796 (1995).
[15] D. Faken and H. Jónsson, Comput. Mater. Sci. **2**, 279 (1994).
[16] R.G. Della Valle, D. Gazzillo, R. Frattini, and G. Pastore, Phys. Rev. B **49**, 12 625 (1994).
[17] Ch. Hausleitner and J. Hafner, Phys. Rev. B **45**, 128 (1992).
[18] R.P. Gupta, Phys. Rev. B **23**, 6265 (1981).
[19] F. Ducastelle, J. Phys. (Paris) **31**, 1055 (1970).
[20] V. Rosato, M. Guillope, and B. Legrand, Philos. Mag. A **59**, 321 (1989).
[21] F. Cleri and V. Rosato, Phys. Rev. B **48**, 22 (1993).
[22] J. Jellinek and I.L. Garzón, Z. Phys. D **20**, 239 (1991).
[23] I.L. Garzón and J. Jellinek, Z. Phys. D **20**, 235 (1991).
[24] I.L. Garzón and J. Jellinek, Z. Phys. D **26**, 316 (1993).
[25] S. Carnalla, A. Posada, and I.L. Garzón, Nanostruct. Mater. **3**, 385 (1993).
[26] M.J. López and J. Jellinek, Phys. Rev. A **50**, 1445 (1994).
[27] L. Verlet, Phys. Rev. **159**, 98 (1967).
[28] J. Mei and J.W. Davenport, Phys. Rev. B **42**, 9682 (1990).
[29] C. Kuiying and L. Qingchun, Chin. Phys. Lett. **9**, 650 (1992).
[30] I.L. Garzón, M. Avalos-Borja, and E. Blaisten-Barojas, Phys. Rev. B **40**, 4749 (1989).
[31] V.A. Likhachev, A.I. Mikhailin, and L.V. Zhigilei, Philos. Mag. A **69**, 421 (1994).
[32] I. Štich, R. Car, and M. Parrinello, Phys. Rev. B **44**, 11 092 (1991).
[33] N. Takeuchi and I.L. Garzón (unpublished).
[34] E. Blaisten-Barojas and H.C. Andersen, Surf. Sci. **156**, 548 (1985).